MANSOURA JOURNAL OF BIOLOGY
Official Journal of Faculty of Science, Mansoura University, Egypt
E-mail: scimag@mans.edu.eg ISSN: 2974-492X

Therapeutic effect of polyvinylpyrrolidone-capped gold nanorods in dimethylbenzene[a]anthracene-induced ovarian cancer in adult femalealbinorat

*Hend Gamal[1,2], Hassan H El-Sayyad, Walid Tawfik, Heba Mohamed Fahmy & Heba A El-Ghaweet[1]**

[1]*Department of Zoology, Faculty of Science,Mansoura University,Mansoura, Egypt*

[2]*Department of Zoology, Faculty of Science,Mansoura University,Mansoura, Egypt*

*** Correspondence to:** *Initials; Hend_Gamal@std.mans.edu.eg , Tel.: +1066986399*

Received: 7/6/2022
Accepted: 21/7/2022

Abstract: The effects of polyvinylpyrrolidone-capped gold nanorods (PVP- capped Au NRs) on ovarian adenocarcinomas in female albino rats induced chemically by 7,12-dimethylbenz[a]anthracene (DMBA) in vivo are investigated in this study. The particles were synthesized by reducing an aqueous solution of gold ions precursor with a chemical reaction. The particles were stabilized against aggregation by PVP. Although the conjugated particles were able to cross the cell membrane and enter the cells via the endocytic route, nothing is known about how PVP- capped Au NRs are transferred. These nanoparticles were described, and 400 µl/rat dosages were given subcutaneously. PVP- capping reduced the amount of gold in various tissues, possibly because of the greater size of capped nanoparticles, which slows the allocation of gold. The ovary underwent histological and immunological examinations. The current findings suggest that PVP-capped Au NRs cross ovarian adenocarcinomas and influence them by inhibiting endothelial cell (EC) viability by binding to vascular endothelial growth factor 165 (VEGF165), a key regulator of endothelial cell function and angiogenesis, and thus decreasing its stimulatory effect, proliferation, and toxicity.

keywords: ovary, cancer, gold nanorods, nanoparticles, DMBA

1.Introduction

The most deadly of all gynecologic cancers is ovarian cancer [1]. When compared to younger women, the incidence of ovarian cancer rises tenfold in the peri- to postmenopausal period [2]. This rise is due in part to three key causes linked to ovarian senescence: oocyte depletion, ovarian steroid production loss, and increased circulating gonadotropic hormones due to the lack of negative feedback from ovarian hormones on the pituitary [2]. As a result, compared to a cycling animal, developing an ovarian cancer animal model in which ovarian failure is caused and the animal is follicle exhausted but preserves remaining ovarian tissue will deliver a model with better physiological relevance. Nanotechnology is a rapidly growing multidisciplinary field that has applications in basic science, industry, and medicine. Various types of nanoparticles (NPs) are used in gene delivery and hushing [1]–[3], drug delivery [4],and cancer treatment [5], [6]. Because gold has historically been thought to be innocuous and biocompatible, gold nanoparticles (AuNPs) are increasingly being used in biomedical research due to their physicochemical qualities and high surface area [7]. AuNPs of various sizes and morphologies have sparked substantial interest in medical applications such as drug delivery [8], as tumor-detector [9], photothermal agent or radiotherapy dose enhancer. These NPs' toxicity is determined by their size, dosage, shape, charge, substance, and surface coating. The effect of PVP capped Au NRs on the and oogenesis is summarized in this paper. Meanwhile, we draw attention to the issues that will need to be researched further in the future [10]. PVP is one of the most important capping agents used in nanotechnology to overcome problems associated with traditional nanoparticle manufacturing processes, such as toxicity, size,

and agglomeration. As a result, PVP is used to create eco-friendly nano formulations with greater application [11], [12]. The current state of knowledge on the effect of PVP capped Au NRs on ovarian structure was discussed in this work. It is discovered that NPs could cause ovarian adenocarcinomas to develop genotoxicity and cytotoxicity. The aim of the present study was to determine the strong influence of PVP capped Au NRs on ovarian adenocarcinomas in vivo, To inform their safe clinical use.

2. MATERIALS AND METHODS

2.1. Animal studies and ethical guidelines

This work followed the National Institute of Health's criteria for the use of laboratory animals (NIH Publication No. 8523, amended 1996), which were approved by Mansoura University's Experimental Animal Ethical Committee. A full of twenty-four female Wister albino rats weighing approximately 100±10 g body weight was obtained from Helwan Breeding Farm, Ministry of Health, Egypt and used for experimentation. Before the experiment, they were given 15 days to acclimate. They were given free access to food and water, and they were kept well-ventilated with a 12-hour light/dark cycle.

2.2.Inductionofovarianadenocarcinmas

This was carried using 7,12-dimethylbenz[a]anthracene (DMBA) (Sigma-Aldrish Company). The most widely used active chemical inductors of mammary carcinogenesis. The applied dose 50 mg/ml is dissolved in 1 ml dimethyl sulfoxide (DMSO, D2650, Sigma) and 4 ml olive oil as previously reported by [13],[14]. One dose was administered subcutaneously, for one week and follow up for 3 weeks.

2.3. Synthesis of gold nanoparticles

2.3.1. Groundwork of colloidal gold nanorods (Au NRs)

Colloidal CTAB capped Au nanorods has been fabricated through seed-mediated method according to previous reports [15]–[17]. Typically, Seed solution from gold nanoclusters were fabricated via chemical reduction of an aqueous solution of gold ions precursor (i.e., 2.5 ml of 1 mM $HAuCl_4.3H_2O$, Au^{3+} ions), in the presence of an aqueous solution of surfactant (i.e., 2.5 ml of 0.2 M of CTAB) using a mild ice cooled reducing agent of sodium borohydride (i.e., 0.6 ml of 0.01 M of $NaBH_4$). Upon the dropwise addition of $NaBH_4$, a reddish-brown colloidal solution is formed that aging for 8 – 12 min under vigorous stirring before injection to growth solution. In addition, A 100 ml of a growth solution was prepared via addition of 1 ml of an aqueous solution of $AgNO_3$ solution to 50 ml of 0.2 M CTAB under vigorous stirring. Then about 50 ml of 1 mM $HAuCl_4.3H_2O$ as gold ions (Au^{3+}) precursor was added under vigorous stirring till a yellowish-brown solution is formed. Finally, an adequate volume of L-ascorbic acid was instantly injected to mixture with gentle shaking till a yellowish-brown color disappears. To fabricate NIR-absorbed gold nanorods, an adequate volume (1.2 ml) of Au^0 seed solution was rapidly injected to growth solution, and the mixture left without any disturbance for 1 hr. The colour of the solution varied over time, showing that the gold nanorods were growing. By centrifugation at 10°C, the produced particles were separated from the growth fluid and the excess CTAB was removed.

2.3.2. Preparation of PVP capped gold nanoparticles

The surface modified gold nanorods with PVP was fabricated as follows [18]; about 5 g of PVP (30K, 0.05 mg/mL) was added to as-purified gold nanorods under vigorous stirring for 2 hr., and kept at room temperature overnight.

2.4. Characterization of gold nanoparticles

The TG-80 twin beam spectrometer was used to record UV-Visible absorption spectra for the prepared samples. The absorbance was measured with a 5 nm increment over the suitable scan range of 200 to 900 nm.

2.4.1. Analysis of zeta potential and zeta average

The surface charge of AuNPs and PVP-AuNPs was determined using a Zeta Potential Analyzer, model Malvern Zeta-size Nano-zs90, made in the United States.

2.4.2. Transmission Electron microscope (TEM) analysis

Size and shape of AuNPs and PVP- capped

AuNPs were examined by TEM (TEM, JEOL JEM-100CX, USA) at Electron Microscope Unit, Mansoura University, Egypt.

2.5. Experimental animals

Twenty-four female Wister albino rats (Rattus norvegicus) weighing approximately 100 g, were divided into 4 groups (n = 6) such as control, PVP- capped Au NRs -treatment, DMBA -treatment, DMBA plus PVP- capped Au NRs. After three weeks induction of ovarian adenocarcinomas using DMBA, treatment was conducted out with PVP- capped Au NRs (400 µl/rat). After one extra-week- treatment, the animals were sacrificed after being killed with chloral hydrate (300mg/kg body weight).

2.5.1 Histological investigation

The specimens were fixed in phosphate buffered formalin (pH7.4) for 10 minutes, dehydrated in increasing grades of ethyl alcohol, cleaned in xylene, and mounted in melted paraplast at 58-62 degrees Celsius.

5 m slices of histological tissue were cut, stained with hematoxylin and eosin, and viewed under a bright field light microscope.

2.5.2 Immunohistochemistry for Caspase-3, Ki-67

On polylysine-coated glass slides, 5 m of formalin-fixed, paraffin-embedded testis samples were mounted. Following that, tissue sections were dewaxed and developed in xylene before being rehydrated in a series of alcohols. To diminish endogenous peroxidase activity, tissue slices were treated in 3 percent H2 O2 for 10 minutes. The tissue sections were treated with the primary monoclonal mouse antibody against caspase-3 (DAKO, clone MIB5, 1:50, mouse) and the primary antibody against (Ki-67) antibody at 1:50 overnight at 4°C in digested medium containing 0.05 percent trypsin (pH 7.8) for 15 minutes at 37°C. After washing, the slides were treated for 50 minutes at room temperature with a secondary biotin-linked anti-mouse antibody, followed by 50 minutes with the streptavidin-peroxidase complex. After that, the sections were washed and developed with diaminobenzidinehydrogen peroxide (DAKO) before being counterstained with hematoxylin. Brown nuclear or cytoplasmic labelling was counterstained with hematoxylin to show the immunological reaction. Negative controls were sections incubated with 1 percent nonimmune serum phosphate buffer solution (PBS) solution. Finally, the histological sections were inspected using a digital Canon camera and an Olympus bright field light microscope. In addition, slides for image analysis were shot with an Olympus® digital camera mounted on an Olympus® microscope with a 1/2 X photo adaptor and a 40 X objective using an Olympus® digital camera positioned on an Olympus® microscope with a 1/2 X photo adaptor. The obtained photos were processed using Video Test morphology® software (Russia) on an Intel® Core 5® based computer, and the percentage area was measured and recorded.

3. RESULTS AND DISCUSSION

3.1. Synthesis and characterization of gold nanorods

Gold nanorods (Au-NRs) have been prepared via wet chemicals based on the seed-mediated method as previously reported [15]–[17].

3.1.1. UV-vis spectrophotometer

The photo-physical and morphological properties have been investigated via UV-vis spectroscopy and transmission electron microscopy techniques, respectively. The absorption spectra exhibited two distinct features were observed at wavelengths of 518 nm, and 713 nm, which due to the presence of crosswise surface plasmon resonance (T-SPR) and longitudinal surface plasmon resonance, respectively. In addition the average calculated aspect ratio was about ~ 3 based on Link et al. formula [19]. This aspect ratio agreed with the average dimensions obtained from TEM image. The average rod length was about 13.25 ± 6.11 nm, while the average rod diameter was about 4.71 ± 1.18 nm (width), and consequently the corresponding aspect ratio was in the range from 3.

3.1.2. Zeta potential

Furthermore, the dynamic light scattering (DLS), and zeta-potential investigated the colloidal stability Au-NRs, as shown in Figure 3. The average hydrodynamic diameter (H_D) was about 77.47 nm with a polydispersity index (PdI) ~ 0.887, and the corresponding zeta potential (ɳ) was about 23.3 mV.

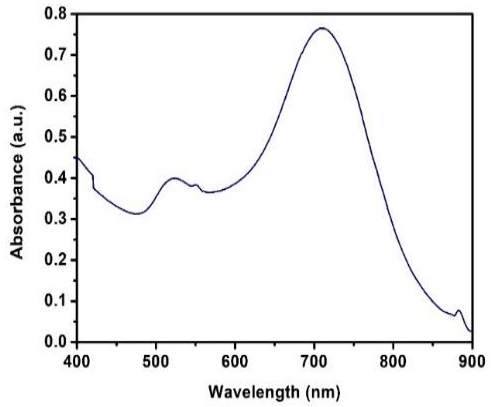

Fig. (1) : UV-Vis absorption spectrum as-prepared Au-NRs

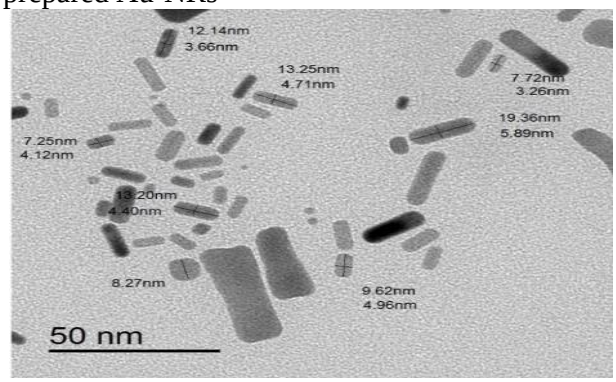

Fig. (2) : TEM images of as prepared Au-NRs

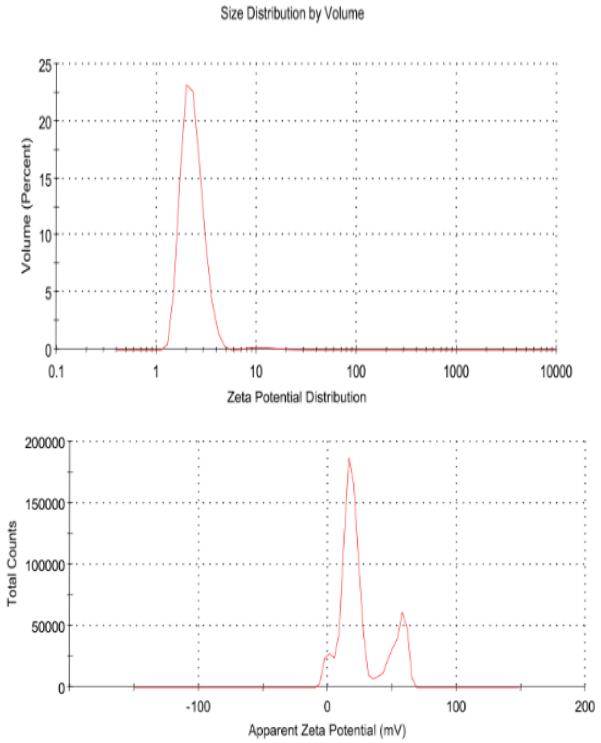

Fig. (3) : DLS (a) and Zeta potential (b) of Au-NRs

3.2. Histopathological observations

In control and PVP- capped Au NRs treated groups, the ovaries possessed normal histological architecture structure with two distinct regions: an outer cortex full of growing follicles and an inner central medulla consisting of loose connective tissue containing blood vessels. The ovarian cortex was coated with germinal epithelium and enclosed underneath by primordial, primary, secondary, mature Graafian follicles. The growing follicles have wide cavities (antrum) full of liquor folliculi and lined by inner zona granulosa cells and outer theca lutein (Fig.4 A, B). Compared with the control and PVP- capped Au NRs -treated groups, the DMBA carcinogenesis group showed a marked increase of degenerated oocytes. Depletion of follicles at all stages of development. Vacuolated ovary in both cortex and medulla (Fig.4 C). In PVP- capped Au NRs -treatment of the DMBA -carcinogenesis group, there was a detected amelioration of the ovarian histological structure. The ovarian sections of DMBA and PVP- capped Au NRs treated rats showed obvious refinement for the previous histopathological findings (Fig.4 D).

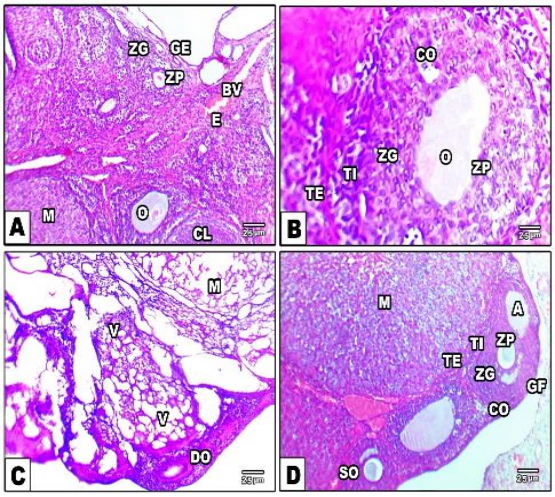

Fig. (4) : Photomicrographs of Histological Cross Section of Rat Ovary. **A.** Control showing active oocytes. **B.** PVP- capped Au NRs positive control showing secondary follicle has wide cavity (antrum) full of liquor folliculi. **C.** DMBA carcinogenesis showing vacuolated ovary and degenerating oocytes. **D.** DMBA carcinogenesis treated with PVP- capped Au NRs showing regenerated oogonial and oocyte cells. Abbreviations; **O**, oocyte; **GE**, germinal epithelium; **BV**, blood vessel; **ZG**, zona granulosa; **ZP**, zona pellucida; **CL**, corpus luteum; **M**, medulla; **E**, epithelial layer; **TI**, theca interna; **TE**, theca externa; **CO**, cumulous oophores; V, vacuoles; **DO**, degenerated oocyte; **GF**, graafian follicle.

3.3. Immunohistochemical Observations

3.3.1. Caspase-3 activity

In group ovarian intoxicated with DMBA carcinogenesis, overexpression of caspase-3 reflecting cell death was observed in the ovarian cells. Administration of PVP- capped Au NRs to the DMBA carcinogenesis group decreased the immunostaining of caspase-3. In addition, caspase-3 staining was elevated in DMBA carcinogenesis ovarian cells with a scattered distribution (Figure 5). Image analysis showed a significant increase of caspase 3 in DMBA carcinogenesis group compared with the other studied groups (Figure 7). Caspase-3 was found in healthy corpora lutea (CL) and theca cells, but not in healthy follicular granulosa cells.

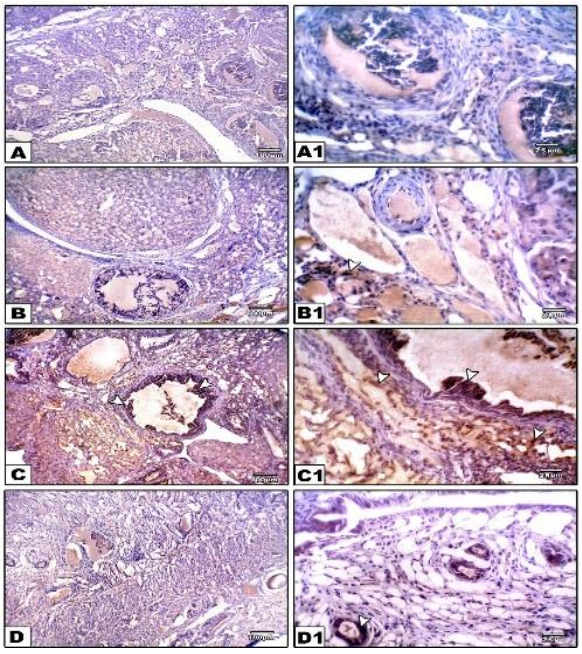

Fig. (5) : Photomicrographs of Formalin Fixed Ovary Immunohistochemical Stain with Caspase-3, control (**A, A1**), PVP- capped Au NRs positive control (**B, B1**), DMBA carcinogenesis (**C, C1**), DMBA carcinogenesis treated with PVP- capped Au NRs (**D, D1**). Note increased immunostaining of Caspase-3 in DMBA carcinogenesis and improved in PVP- capped Au NRs -treated studied groups. Also, caspase-3 was found in healthy corpora lutea (CL) luteal cells and theca, but not in healthy follicular granulosa cells. The degree of caspase-3 immunoreactivity is shown by the arrow heads.

3.3.2. Ki-67 activity

Ki-67 immunohistochemistry revealed higher immunostaining in the DMBA carcinogenesis group, indicating greater proliferative activity. However, when Au NRs were treated with PVP, the Ki-67 immunohistochemical reactivity was reduced (Figure 6). Following image analysis, Ki-67 showed a significant increase in the immune reaction in the DMBA carcinogenesis compared with the other studied groups (Figure7).

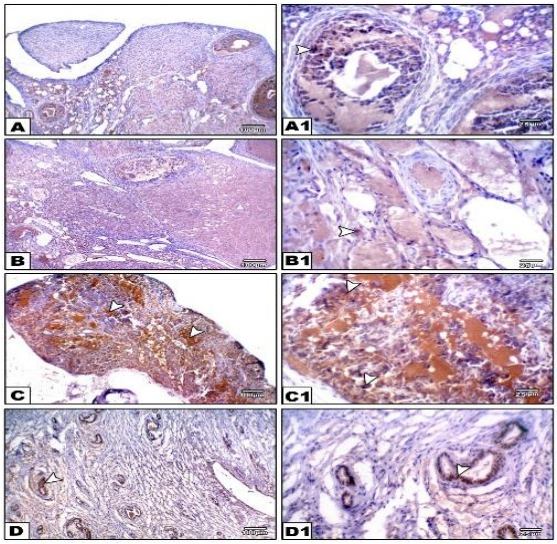

Fig. (6) : Photomicrographs of Formalin Fixed Ovary Immunohistochemical Stain with Ki-67, control (**A, A1**), PVP- capped Au NRs positive control (**B, B1**), DMBA carcinogenesis (**C, C1**), DMBA carcinogenesis treated with PVP- capped Au NRs (**D, D1**). Also note remarkable overexpression of Ki-67 in DMBA carcinogenesis and improved in PVP- capped Au NRs -treated studied groups. The arrows heads indicate the degree of Ki-67 immunoreactivity.

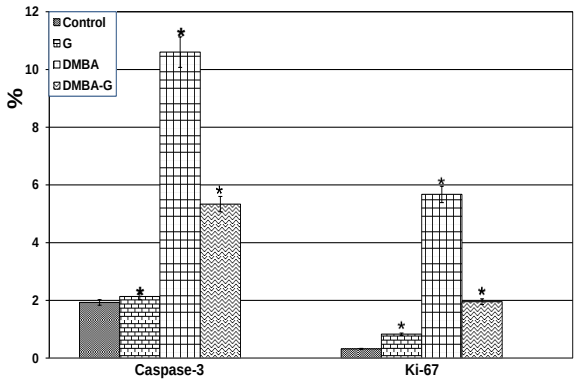

Fig. (7) : Image Analysis of Female Ovary Subjected to DMBA Carcinogenesis and Treated with PVP- capped Au NRs. In both DMBA carcinogens and PVP-capped Au NRs -treatment, Caspase-3 expressing apoptosis showed a considerable rise in image analysis. Ki-67 reflecting proliferative activity showing significant increase image analysis in both DMBA

carcinogens and DMBA carcinogens and PVP-capped Au NRs -treatment. Star means significant at P ‹ 0.05.

4. Discussion

For greater medication accumulation at tumor locations, nanoparticles can rely more on the higher permeability and retention effect generated by leaky tumor vasculatures in cancer treatments [20]. The expression of stem cell markers was discovered to be inhibited by gold nanoparticles (AuNPs), and the pool of stem cell phenotype (SP) cells was reported to be reduced. Exploring the signaling pathways that control AuNP-mediated stemness inhibition will aid in identifying important actors implicated in drug resistance [21]. In this study, we persuaded ovarian cancer by injecting DMBA subcutaneously of female Wistar rats. We have detected ovarian adenomas or adenocarcinomas following revelation of ovarian tissue to DMBA chemical carcinogenesis administered by the technique of KATO et al. (1973). Follicular destruction precedes follicular cell proliferation and neoplasia in the mouse ovary, which is analogous to the action of a variety of carcinogens [23], [24]. As a result, tumor formation may be linked to follicular tissue disturbance rather than rupture of the surface epithelium. In this rat model, rats were given either PVP-capped gold nanorods (treatment group) or no PVP-capped gold nanorods (control group) to see if PVP-capped Au NRs could prevent ovarian cancer. The new induction strategy raised the incidence of ovarian cancer in a shorter induction period, according to our findings. The treatment with PVP-capped Au NRs reduced tumor incidence, inhibited tumor growth, and increased the survival of tumor-bearing rats. In ovarian cancer cells, the proliferative inhibitory impact of PVP-capped Au NRs was linked to enhanced apoptosis. Animal models that mimic the pathophysiological aspects of human ovarian cancer are critical for understanding the disease's origin and generating new therapeutic approaches [25]–[27]. Multicellular organisms use apoptosis to eliminate undesirable cells and maintain cellular balance. Caspases are critical mediators of programmed apoptosis and serve as markers of apoptosis [28] . Among them, Caspase-3 is a frequently activated death protease that catalyzes the exact cleavage of many important cellular proteins, making it an influential apoptotic marker. The discovery of endogenous caspase-3 in luteal but not granulosa cells shows that the former simply requires a signal to induce DNA degradation, whereas the latter requires both caspase-3 expression and a signal. Apoptosis expression in follicular granulosa cells could indicate ovulation cycle disruption. Many studies have suggested that an increased incidence of apoptotic cells in the follicular granulosa is a sign of the pre-ovulatory process and the subsequent early luteinization process, which results in infertility [29]–[31]. Ki-67 was discovered to be a nuclear non-histone protein by Gerdes et al. Due to its total expression in proliferating tissues and absence in quiescent cells, Ki-67 expression was of significant interest to identify as a marker of cell proliferation. The Ki-67 gene is found on human chromosome 10's long arm (10q25). Ki-67 is also used as a potential active intermediate or substitute marker of treatment efficacy, both as a fixed marker of proliferative activity and with numerous assessments during therapy [32]–[34]. Enhanced caspase-3 and Ki-67 immunohistochemistry were used to examine the increased inflammation in DMBA ovarian adenocarcinomas. The degree of inflammation was eased by PVP-capped Au NRs - treatment of the DMBA. Our findings revealed that the DMBA-induced ovarian cancer rat model exhibited some characteristics like those seen in ovarian cancer patients. During ovarian cancer, cells shed into the ascites and metastasize locally, primarily to the omentum, peritoneal wall, diaphragm, and small bowel mesentery. This diffuse metastasis was also seen in this study's rat model. Ascites is linked to a poor prognosis in late-stage cancer patients. At a later stage, these rats developed abdominal bulk and bloody ascites, as well as weight defeat and cachexia. This is also seen in people with ovarian cancer. Furthermore, our findings and earlier research revealed that the majority of tumors that grew in this rat model were adenocarcinomas [35]–[37], a prominent pathogenic subtype of ovarian cancer in humans. Several pathogenic aspects of human ovarian cancer are mimicked in this rat model. There are many issues that

need to be solved further in the future. The factors that affect GNP pharmacokinetics, biodistribution, and in vivo toxicity.

5. Conclusion

It has been discovered that exposing adult female albino rats to gold nanoparticles leads to metal deposition at many sites, as well as to histological changes. This was accomplished by decreasing endothelial cell (EC) viability by binding to vascular endothelial growth factor 165 (VEGF165), a key regulator of endothelial cell function and angiogenesis. This binding reduces VEGF165's stimulatory action, proliferation, and toxicity.

Acknowledgment Conclusion

6. REFERENCES

1. P. T. Yang, L. Hoang, W. W. Jia, and E. D. Skarsgard, (2011) "In utero gene delivery using chitosan-DNA nanoparticles in mice," *J. Surg.* Res., vol. **171**, no. 2, pp. 691–699,.
2. Q. Xu, T. Zhang, Q. Wang, X. Jiang, A. Li, Y. Li, T. Huang, F. Li, Y. Hu, D. Ling, J. Gao, (2018) "Uniformly sized iron oxide nanoparticles for efficient gene delivery to mesenchymal stem cells," *Int. J. Pharm.*, vol. **552**, no. 1–2, pp. 443–452,.
3. Q. Yu, Y. Qiu, X. Wang, J. Tang, Y. Liu, L. Mei, M. Li, M. Yang, L. Tang, H. Gao, Z. Zhang, W. Xu, Q. He, (2018) "Efficient siRNA transfer to knockdown a placenta specific lncRNA using RGD-modified nano-liposome: A new preeclampsia-like mouse model," *Int. J. Pharm.*, vol. **546**, no. 1–2, pp. 115–124,.
4. L. Kou, R. Sun, V. Ganapathy, Q. Yao, and R. Chen, (2018) "Recent advances in drug delivery via the organic cation/carnitine transporter 2 (OCTN2/SLC22A5)," Expert Opin. Ther. Targets, vol. **22**, no. 8, pp. 715–726,.
5. M. Benguigui, I. Weitz, M. Timaner, T. Kan, D. Shechter, O. Perlman, S. Sivan, Z. Raviv, H. Azhari, Y. Shaked, (2019) "Copper oxide nanoparticles inhibit pancreatic tumor growth primarily by targeting tumor initiating cells," Sci. Rep., vol. **9**, no. 1, pp. 1–10,.
6. E. Niza, C. Jiménez, M. López, I. Bravo, J. Osma, F. Martínez, M. Buchaca, I. Posadas, J. Vázquez, A. Sanchez, D. Merino, E. Solano, A. Ocaña, C. Moreno, "Poly(2019) (Cyclohexene phthalate) nanoparticles for controlled dasatinib delivery in breast cancer therapy," Nanomaterials, vol. **9**, no. 9, p. 1208,.
7. A. Liu and B. Ye, (2013) "Application of gold nanoparticles in biomedical researches and diagnosis.," Clin. Lab., vol. **59**, no. 1–2, pp. 23–36,.
8. J. D. Gibson, B. P. Khanal, and E. R. Zubarev, (2007) "Paclitaxel-functionalized gold nanoparticles," *J. Am. Chem. Soc.*, vol. **129**, no. 37, pp. 11653–11661,.
9. B. J. Tromberg, A. Orenstein, S. Kimel, S. J. Barker, J. Hyatt, J. S. Nelson, M. W. Berns, (1990) "In vivo tumor oxygen tension measurements for the evaluation of the efficiency of photodynamic therapy," Photochem. Photobiol., vol. **52**, no. 2, pp. 375–385,.
10. C.-C. Hou and J.-Q. Zhu, (2017) "Nanoparticles and female reproductive system: how do nanoparticles affect oogenesis and embryonic development," Oncotarget, vol. **8**, no. 65, p. 109799,.
11. M. Goodarz Naseri, E. Saion, and N. Khalil Zadeh, (2013) "The amazing effects and role of PVP on the crystallinity, phase composition and morphology of nickel ferrite nanoparticles prepared by thermal treatment method," Int. nano Lett., vol. **3**, no. 1, pp. 1–8,.
12. G. Pandey, S. Singh, and G. Hitkari, (2018) "Synthesis and characterization of polyvinyl pyrrolidone (PVP)-coated Fe3O4 nanoparticles by chemical co-precipitation method and removal of Congo red dye by adsorption process," Int. Nano Lett., vol. **8**, no. 2, pp. 111–121,.
13. M. F. Dias, E. Sousa, and C. F. Oliveira, (2000) "Induced Mammary Tumors in Rats by a Combined Regimen," no. **3**, pp. 3–8,.
14. M. M. Soliman and A. M. S. Elfeky, (2016) "Studies on the biochemical and molecular effects of some natural herbs on experimental-induced breast cancer in Wistar rats," *Natl. J. Physiol. Pharm. Pharmacol.*, vol. **6**, no. 5, pp. 349–358, ,

doi:
10.5455/njppp.2016.6.200220160428002.
15. B. Nikoobakht and M. A. El-Sayed, (2003). “Preparation and growth mechanism of gold nanorods (NRs) using seed-mediated growth method,” Chem. Mater., vol. **15**, no. 10, pp. 1957–1962,
16. C. J. Johnson, E. Dujardin, S. A. Davis, C. J. Murphy, and S. Mann, (2002) “Growth and form of gold nanorods prepared by seed-mediated, surfactant-directed synthesis,” *J. Mater. Chem.*, vol. **12**, no. 6, pp. 1765–1770,.
17. A. N. Emam, M. B. Mohamed, E. Girgis, and K. V. Rao, (2015) “Hybrid magnetic–plasmonic nanocomposite: embedding cobalt clusters in gold nanorods,” RSC Adv., vol. **5**, no. 44, pp. 34696–34703,.
18. K. I. Requejo, A. V Liopo, and E. R. Zubarev, (2018) “Synthesis of Gold Nanorods Using Poly (vinylpyrrolidone) of Different Molecular Weights as an Additive,” ChemistrySelect, vol. **3**, no. 43, pp. 12192–12197,.
19. S. Link, M. B. Mohamed, and M. A. El-Sayed, (1999) “Simulation of the optical absorption spectra of gold nanorods as a function of their aspect ratio and the effect of the medium dielectric constant,” *J. Phys. Chem. B*, vol. **103**, no. 16, pp. 3073–3077,.
20. R. Agarwal and S. B. Kaye, (2003) “Ovarian cancer: strategies for overcoming resistance to chemotherapy,” Nat. Rev. Cancer, vol. **3**, no. 7, pp. 502–516,.
21. X. Xiong, R. Arvizo, S. Saha, D. Robertson, S. McMeekin, R. Bhattacharya, P. Mukherjee, (2014) “Sensitization of ovarian cancer cells to cisplatin by gold nanoparticles,” Oncotarget, vol. **5**, no. 15, p. 6453,.
22. T. Kato, M. Yakushiji, A. Tsunawaki, and K. Ide, , (1973) “A study of experimental ovarian tumors produced in rats by the chemical carcinogen, 20-methylcholanthrene,” *Kurume Med. J.*, vol. **20**, no. 3, pp. 159–167.
23. I. Kuwahara, (1967) “Experimental induction of ovarian tumors in mice treated with single administration of 7, 12-dimethylbenz [a] anthracene, and its histopathological observation,” *GANN Japanese J. Cancer* Res., vol. **58**, no. 3, pp. 253-266_5,.
24. T. Krarup, , (1969). “Oocyte destruction and ovarian tumorigenesis after direct application of a chemical carcinogen (9: 10-dimethyl-1: 2-benzanthrene) to the mouse ovary*,” Int. J. cancer*, vol. **4**, no. 1, pp. 61–75
25. A. A. Khan, M. Jabeen, A. A. Khan, and M. Owais, (2013) “Anticancer efficacy of a novel propofol–linoleic acid-loaded escheriosomal formulation against murine hepatocellular carcinoma,” Nanomedicine, vol. **8**, no. 8, pp. 1281–1294,.
26. A. A. Khan, A. M. Alanazi, M. Jabeen, I. Hassan, and M. A. Bhat, , (2016). “Targeted nano-delivery of novel omega-3 conjugate against hepatocellular carcinoma: Regulating COX-2/bcl-2 expression in an animal model,” Biomed. Pharmacother., vol. **81**, pp. 394–401
27. P. J. Morin and A. T. Weeraratna, (2016) “Genetically-defined ovarian cancer mouse models*,” J. Pathol.*, vol. **238,** no. 2, pp. 180–184,.
28. M. Los, S. Wesselborg, and K. Schulze-Osthoff, (1999) “The role of caspases in development, immunity, and apoptotic signal transduction: lessons from knockout mice,” Immunity, vol. **10**, no. 6, pp. 629–639,.
29. K. Kugu et al., (1998) “Analysis of apoptosis and expression of bcl-2 gene family members in the human and baboon ovary,” Cell Death Differ., vol. **5**, no. 1, pp. 67–76,.
30. T. Matikainen et al., (2001). “Caspase-3 gene knockout defines cell lineage specificity for programmed cell death signaling in the ovary,” Endocrinology, vol. **142**, no. 6, pp. 2468–2480,
31. N. S. Abadeer and C. J. Murphy, -(2016) “Recent Progress in Cancer Thermal Therapy Using Gold Nanoparticles,” *Journal of Physical Chemistry C*, vol. **120**, no. 9. American Chemical Society, pp. 4691–4716, 10-Mar.
32. E. Endl and J. Gerdes, (2000) “The Ki-67 protein: fascinating forms and an unknown function,” Exp. Cell Res., vol. **257**, no. 2, pp. 231–237,.

33. K. Kritpracha, J. Hanprasertpong, V. Chandeying, C. Dechsukhum, and A. Geater, (2005) "Survival analysis in advanced epithelial ovarian carcinoma in relation to proliferative index of MIB-1 immunostaining," *J. Obstet. Gynaecol*. Res., vol. **31**, no. 3, pp. 268–276,.
34. G. Aune, A. K. Stunes, S. Tingulstad, Ø. Salvesen, U. Syversen, and S. H. Torp, (2011) "The proliferation markers Ki-67/MIB-1, phosphohistone H3, and survivin may contribute in the identification of aggressive ovarian carcinomas," *Int. J. Clin. Exp. Pathol*., vol. **4**, no. 5, p. 444,.
35. K. A. Crist et al., (2005) "Characterization of rat ovarian adenocarcinomas developed in response to direct instillation of 7, 12-dimethylbenz [a] anthracene (DMBA) coated suture," Carcinogenesis, vol. **26**, no. 5, pp. 951–957,.
36. A. A. Khan, (2017) "Pro-apoptotic activity of nano-escheriosome based oleic acid conjugate against 7, 12-dimethylbenz (a) anthracene (DMBA) induced cutaneous carcinogenesis," Biomed. Pharmacother., vol. **90**, pp. 295–302,.
37. Y. Huang, W. Jiang, Y. Wang, Y. Zheng, Q. Cong, and C. Xu, (2012) "Enhanced efficacy and specificity of epithelial ovarian carcinogenesis by embedding a DMBA-coated cloth strip in the ovary of rat*," J. Ovarian* Res., vol. **5**, no. 1, pp. 1–8,.